Supplemental Information

Fitting of Dispersion Profiles

Relaxation dispersion data for both G48M and G48V mutants of the Fyn SH3 domain were recorded as described in Methods. A series of 10 to 15 2D spectra at different CPMG frequencies, ν_{CPMG}, (typically including 3 duplicate spectra) were collected for each mutant at each temperature and magnetic field strength using a pulse sequence described elsewhere.[1] Spectra were recorded with a constant relaxation delay T_{CP} = 40 ms (30 ms for G48V at 10°C, 800 MHz) along with a single reference spectrum, T_{CP} = 0, as described previously.[1] The intensities of the cross peaks were converted into effective relaxation rates, R_2^*, via

$$R_2^*(\nu_{CPMG}) = -\frac{1}{T_{CP}} \ln \frac{I_1(\nu_{CPMG})}{I_0} \qquad \text{(A1)}$$

where $I_1(\nu_{CPMG})$ is the peak intensity in the spectrum recorded with a non-zero T_{CP} value at a given ν_{CPMG} frequency, and I_0 is the peak intensity in the reference spectrum. Uncertainties in R_2^* were calculated as:

$$\Delta R_2^*(\nu_{CPMG}) = \frac{1}{T_{CP}} \frac{<\Delta I_1>}{I_1(\nu_{CPMG})} \qquad \text{(A2)}$$

where $<\Delta I_1>$ is the average standard deviation of the peak intensity estimated from repeat measurements. In cases where calculated errors were less than 2% of R_2^*, a minimum value of 2% was used. The resulting dispersion profiles $R_2^*(\nu_{CPMG})$ include 10 to 15 points with ν_{CPMG} frequencies ranging from 50 to 1000 Hz.

Dispersion profiles for each residue were considered for subsequent computations only if for all temperatures (i) an F-test analysis showed that the fit using a two-state exchange model (χ^2_{exch}) gives significant improvement (p < 0.1%) over one which neglects exchange (χ^2_{simple}), and $P(\chi^2_{exch}) > 0.1\%$, $P(\chi^2_{simple}) < 0.1\%$, (ii) the difference in effective relaxation rates, R_2*, measured at the lowest and highest CPMG frequencies used are greater than 3 s^{-1} and (iii) uncertainties of less than 10% in each R_2* value comprising the dispersion profile are obtained. In this way 23(26) residues were selected for G48M(G48V).

Theoretical values of $R^{*}_{2,clc}$ were calculated according to

$$R^{*}_{2,clc} = -\frac{1}{4n\delta}\ln\frac{M_F(4n\delta)}{M_F(0)} \qquad \text{(A3)}$$

where,

$$\mathbf{M}(4n\delta) = \left(\exp(\mathbf{A}\delta)\exp(\tilde{\mathbf{A}}\delta)\exp(\tilde{\mathbf{A}}\delta)\exp(\mathbf{A}\delta)\right)^{n}\mathbf{M}(0), \qquad \text{(A4)}$$

$T_{CP} = 4n\delta$ with $2n$ the number of 180° pulses within the T_{CP} period, $\mathbf{M}(t)$ is the magnetization vector given by $(M_F(t), M_U(t))^{\mathrm{T}}$ in the case of 2-site exchange between states F and U and by $(M_F(t), M_I(t), M_U(t))^{\mathrm{T}}$ in the case of 3-site exchange between F, I and U, $\mathbf{M}(0)$ is the vector of initial magnetization equal to $(p_F, p_U)^{\mathrm{T}}$ and $(p_F, p_I, p_U)^{\mathrm{T}}$ for 2- and 3-site exchange processes, respectively, where p_F, p_I and p_U are the populations of the exchanging states. In the case of 2-site exchange between F and U, the 2×2 evolution matrices $\mathbf{A}$ and $\tilde{\mathbf{A}}$ are given by:

$$\mathbf{A} = \begin{pmatrix} -R_{2F} - k_{FU} & k_{UF} \\ k_{FU} & -R_{2U} - k_{UF} + i\Delta\omega_{FU} \end{pmatrix}, \qquad \text{(A5)}$$

$$\tilde{\mathbf{A}} = \begin{pmatrix} -R_{2F} - k_{FU} & k_{UF} \\ k_{FU} & -R_{2U} - k_{UF} - i\Delta\omega_{FU} \end{pmatrix},$$

where k_{kl} is the rate constant for the transition from state k to l, $\Delta\omega_{kl}$ is the frequency difference between states k and l, $R_{2,k}$ is the transverse relaxation rate for spins in state k, the symbol '~' denotes 'complex conjugate' and $i = \sqrt{-1}$. In the case of 3-site exchange between states F, I and U, the 3×3 evolution matrices $\mathbf{A}$ and $\tilde{\mathbf{A}}$ are given by:

$$\mathbf{A} = \begin{pmatrix} -R_{2F} - k_{FI} & k_{IF} & 0 \\ k_{FI} & -R_{2I} - k_{IF} - k_{IU} + i\Delta\omega_{FI} & k_{UI} \\ 0 & k_{IU} & -R_{2U} - k_{UI} + i\Delta\omega_{FU} \end{pmatrix}, \qquad \text{(A6)}$$

$$\tilde{\mathbf{A}} = \begin{pmatrix} -R_{2F} - k_{FI} & k_{IF} & 0 \\ k_{FI} & -R_{2I} - k_{IF} - k_{IU} - i\Delta\omega_{FI} & k_{UI} \\ 0 & k_{IU} & -R_{2U} - k_{UI} - i\Delta\omega_{FU} \end{pmatrix}.$$

For the purpose of minimization of the target function (see below) we recast the evolution matrices $\mathbf{A}$ and $\tilde{\mathbf{A}}$ in terms of the exchange rate constants, $k^{ex}_{kl} = k_{kl} + k_{lk}$, and populations of the exchanging states, p_k, ($\sum_k p_k = 1$), which can be related to the rate constants k_{kl} using the condition of microscopic reversibility, $p_k k_{kl} = p_l k_{lk}$. No direct transitions were allowed between

states F and U in the 3-site F↔I↔U model, so the rate constant $k_{FU}^{ex} = k_{FU} + k_{UF}$ in this model was set to zero. In A5 and A6 above, values of R_{2F}, R_{2U} and R_{2I} were set equal; although this assumption is almost certainly an oversimplification, it introduces little error into the extracted exchange parameters so long as $p_F >> p_I, p_U$, as is the case here.[2]

The data for a select set of n_n residues collected at n_t temperatures and n_f(T) magnetic fields was analyzed together under the assumption that (i) all residues have the same exchange rate constants, with the temperature dependence of the rate constants described by transition-state theory, $ln(k_{kl}) = ln(k_bT/h) + \Delta S^+/R - \Delta H^+/RT$, where ΔS^+ and ΔH^+ are activation entropies and enthalpies, k_b is Boltzman's constant, h is Plank's constant, and that (ii) the chemical shift differences between the exchanging states are independent of temperature. Thus, the 2-site exchange model, F↔U, includes $\{\sum_T n_n n_f(T)\} + n_n + 4$ adjustable parameters ($n_n n_f$(T) values of $R_2 = R_{2,F} = R_{2,U}$ for each of n_t temperatures, n_n values of $\Delta\varpi_{FU} = \Delta\omega_{FU}/\omega_N$, where ω_N is Larmour frequency of the ^{15}N nuclei, ΔH_{FU}^+, ΔS_{FU}^+, ΔH_{UF}^+ and ΔS_{UF}^+) and the 3-site model F↔I↔U includes $\{\sum_T n_n n_f(T)\} + 2n_n + 8$ parameters ($n_n n_f$(T) values of $R_2 = R_{2,F} = R_{2,I} = R_{2,U}$ for each of n_t temperatures, n_n values of $\Delta\varpi_{FI}$, n_n values of $\Delta\varpi_{FU}$, ΔH_{FI}^+, ΔS_{FI}^+, ΔH_{IF}^+, ΔS_{IF}^+, ΔH_{IU}^+, ΔS_{IU}^+, ΔH_{UI}^+, ΔS_{UI}^+).

Values of model parameters were extracted by least-square fits of the experimental R_2^* rates to the theoretical values, $R_{2,clc}^*$. The fits were performed by minimization of a χ^2 target function given by

$$\chi^2(\zeta) = \sum \frac{\left(R_{2,clc}^*(\zeta) - R_2^*\right)^2}{\left(\Delta R_2^*\right)^2}, \qquad \text{(A7)}$$

where $\zeta = \{x_1,\ldots,x_{npar}\}$ denotes the set of adjustable model parameters. The summation in eq A7 runs over the experimental data. If the errors in the experimental data are small, normally distributed and uncorrelated with each other, $\chi^2(\zeta)$ at its minimum is given by a χ^2 distribution function with $\nu = n_{dat}$-n_{par} degrees of freedom, where n_{dat} is the number of experimental data points and n_{par} is the number of adjustable model parameters. Note that for ν > 20-30 the χ^2 distribution is well approximated by a normal distribution centered at ν having a mean square deviation of $\sqrt{2\nu}$.[3] Choosing between the alternative models described above (*i.e.*, between 2-

and 3-site models) was based on F-test statistics.[3] In the case of models with high ν values, the addition of further adjustable parameters is justified only by a reduction of $\chi^2(\zeta)$ that significantly exceeds the difference in numbers of degrees of freedom between the two models. Uncertainties of the adjustable model parameters $\zeta = \{x_1,\ldots,x_{npar}\}$ were estimated using the covariance matrix method[4], which exploits the properties of $\chi^2(\zeta)$ at its minimum. In contrast to other approaches for estimating errors, such as extensive Monte-Carlo, jackknife or bootstrap simulations involving multiple minimizations of $\chi^2(\zeta)$ with different data sets, the covariance matrix method is computationally much less demanding as it requires an estimate of the matrix of second derivatives of $\chi^2(\zeta)$ with respect to fitting parameters, x_1, only once. This is particularly advantageous for problems like the one here, where optimization of $\chi^2(\zeta)$ is performed with thousands of experimental data points and hundreds of adjustable parameters, so that one minimization run may take several hours.

Finally, once the rates defining the exchange process and their temperature dependence were obtained, additional residues (*i.e.* those with $p < 0.1\%$ and $P(\chi^2_{simple}) < 0.1\%$, above) were included in the analysis (for a total of 37 and 40 residues for G48M and G48V) to obtain chemical shift differences, keeping rates and thermodynamic parameters fixed.

Structure Calculations

In order to obtain structures for which $\Delta^{calc}=\Delta^{exp}$ we used a simulation protocol similar to that used to determine structures of native states using conventional restraints derived from NMR experiments, such as nOes, ^{3}J values and residual dipolar couplings.

Initial model of N: For each mutant of the Fyn SH3 domain a model of the native state was obtained based on the crystal structure of the wild type protein (pdb code 1shf[5]). The models were constructed by modification of G48 to either M48 or V48 using the program MOLDEN[6] followed by an energy minimization (steepest descent, 300 steps). The force-field used in all simulations was CHARMM19 with an implicit representation of the solvent.[7] The simulations were carried out in CHARMM (release c30a1).

Interpretation of the chemical shifts: We assumed that ^{15}N chemical shifts depend mostly on the tertiary interactions of the N atom, which can involve hydrogen bonding.[8] We thus have adopted the following expression for the calculation of Δ^{calc} from the structures generated during the simulations,

$$\Delta^{calc}(i) = \frac{N_{FS}(i)}{N_{FU}(i)} = \frac{N_F(i) - N_S(i)}{N_F(i) - N_U(i)} \qquad \text{(A8)}$$

where $N_S(i)$ is the number of native contacts formed by the amide nitrogen of residue *i* in conformation S at a given time in the simulations. This number is calculated as

$$N_S(i) = \sum_k^M \psi(r_{jk} - r_c)\lambda_{jk} \qquad \text{(A9)}$$

where *j* represents the backbone N atom of residue *i*, *k* runs over all heavy atoms of the protein (M) and λ_{jk} is equal to one when *j* and *k* are less than 6.5 Å in the native state and belong to residues which are more than two positions apart in the primary structure (otherwise λ_{jk} = 0), and the function ψ(r) is a smoothed step function (β = 5 Å^{-1}, r_c = 6.5Å),

$$\psi(r) = \frac{1}{1 + e^{\beta r}} \ . \qquad \text{(A10)}$$

For the structure calculations presented here we have used $N_U(k)$ = 0. Residues were only included in the calculations if the chemical shift of the I state was between that of the U and F states (corresponding to 54% and 58% of the residues considered in G48M, G48V). 92%(78%) of the I shifts were either between U and F or within 1 ppm of U and F in G48M(G48V).

Initial model of I: An initial model for the I state of each mutant was obtained using Biased Molecular Dynamics (BMD)[9]. This is a method to carry out restrained simulations in which the system is biased to follow a trajectory that leads to a structure which fulfils the restraints and is particularly useful in cases where the interpretation of the restraints is not straightforward. The BMD method was implemented during a 2 ns simulation starting from an equilibrated model of the native state of each mutant (obtained after 1 ns of unrestrained Molecular Dynamics). During the simulations the following pseudo-energy term was added to the CHARMM19 force-field,

$W = \frac{\alpha}{2}\rho^2$, if $\rho(t) \geq \rho_a$

$W = 0$, if $\rho(t) < \rho_a$,

$$\rho(t) = \frac{1}{N_\Delta} \sum_{i \in E} \left(\Delta^{calc} - \Delta^{\exp} \right)^2, \qquad \text{(A11)}$$

$\rho_a = \min \rho(\tau)$, $0 \leq \tau \leq t$

and N_Δ is the number of restraints used in the simulations, E is the ensemble of residues from which restraints were available and α is doubled during a series of 10 steps to a final value of 5.10^6 kcal.mol^{-1}.

Generation of the ensembles: Once a first configuration that fulfilled the restraints had been obtained by Biased Molecular Dynamics a simulated annealing protocol was used to sample the conformational space compatible with the restraints. The potential, $W = \frac{\alpha}{2}\rho^2$, was used with the value of α set to 5.10^6 kcal.mol^{-1} in each step of the simulated annealing protocol and the temperature of the system was increased in 10K steps from 300 to 450K (during 150 ps) in order to maximize sampling. The temperature was then gradually decreased to 300K (during 0.75 ns), after which the configuration of the system was saved for analysis. Each structure determination consisted of 25 of such cycles and hence yielded 25 structures. The initial model of I obtained by Biased Molecular Dynamics was used as the starting structure of cycle 1 and the structure from cycle *i* was used as the starting structure of cycle *i+1*. At the end of each cycle one structure was saved and added to the ensemble representing the I state.

Cross-validation of the ensembles: In order to assess the reliability of our interpretation of the chemical shifts and of the overall structure determination procedure the structure determinations were repeated after removal of some of the restraints; the ensemble-averaged Δ^{calc} of the unrestrained residues were then compared to Δ^{exp}. The Pearson correlation coefficient was, respectively for the two mutants, $\rho^{G48M} = 0.80$ (using 9 restraints and predicting the remaining 11) and $\rho^{G48V} = 0.83$ (using 14 restraints and predicting the remaining 9).

Table 1S. Folding kinetics parameters obtained from a global fit of CPMG dispersion data for Fyn SH3 mutants. The data for 23(26) residues of G48M(G48V) recorded at 5(4) temperatures and 3(2) magnetic fields were fit together using a 3-site exchange model (see Methods for the details of data fitting). The rate constants for transitions between F, I and U states are assumed to follow transition state theory (with $\Delta C_P = 0$). For comparison we also show the folding and unfolding rate constants at 25 °C calculated using a 2-site model from NMR dispersion data and the values obtained from stopped-flow measurements.[10] (k_f,k_u) values of (78±4,0.06±0.01)s^{-1} are obtained for WT Fyn-SH3 at 25°C from stopped-flow experiments.

G48M									
3-site	Temp [°C]	k_{FI} [s^{-1}]	k_{IF} [s^{-1}]	k_{IU} [s^{-1}]	k_{UI} [s^{-1}]	$k_{FI} + k_{IF}$ [s^{-1}]	$k_{IU} + k_{UI}$ [s^{-1}]	p_I [%]	p_U [%]
	15	6.2 ± 0.3	586 ± 49	834 ± 85	1204 ± 102	593 ± 25	2038 ± 172	1.03 ±0.04	0.72 ± 0.04
	20	11.1 ± 0.6	954 ± 83	1613 ± 138	1549 ± 123	965 ± 48	3161 ± 215	1.14 ± 0.05	1.18 ± 0.05
	25	19.6 ± 1.2	1526 ± 149	3050 ± 283	1976 ± 188	1546 ± 103	5026 ± 336	1.24 ± 0.06	1.92 ± 0.07
	30	34.0 ± 2.5	2405 ± 269	5650 ± 666	2501 ± 305	2439 ± 211	8151 ± 648	1.35 ± 0.08	3.05 ± 0.10
	35	57.9 ± 5.2	3737 ± 480	10262 ± 1548	3144 ± 484	3795 ± 407	13405 ± 1342	1.45 ± 0.11	4.75 ± 0.13
2-site		NMR				Stop Flow			
	Temp [°C]	k_{FU} [s^{-1}]	k_{UF} [s^{-1}]	$k_{FU} + k_{UF}$ [s^{-1}]	p_U [%]	k_{FU} [s^{-1}]	k_{UF} [s^{-1}]	$k_{FU} + k_{UF}$ [s^{-1}]	p_U [%]
	25	15.8 ± 0.1	516 ± 7	532 ± 7	2.97 ± 0.04	17.8 ± 7.8	453 ± 101	471 ± 101	3.78 ± 0.81
G48V									
3-site	Temp [°C]	k_{FI} [s^{-1}]	k_{IF} [s^{-1}]	k_{IU} [s^{-1}]	k_{UI} [s^{-1}]	$k_{FI} + k_{IF}$ [s^{-1}]	$k_{IU} + k_{UI}$ [s^{-1}]	p_I [%]	p_U [%]
	10	22.3 ± 0.8	1081 ± 69	1061 ± 80	730 ± 41	1103 ± 69	1791 ± 105	1.97 ± 0.10	2.86 ± 0.09
	15	33.8 ± 1.3	1667 ± 111	1805 ± 112	988 ± 57	1701 ± 111	2793 ± 145	1.92 ± 0.09	3.50 ± 0.09
	20	50.4 ± 2.3	2535 ± 188	3017 ± 199	1324 ± 96	2586 ± 190	4341 ± 267	1.87 ± 0.09	4.25 ± 0.09
	25	74.1 ± 4.1	3803 ± 325	4957 ± 413	1758 ± 164	3877 ± 329	6715 ± 545	1.81 ± 0.09	5.12 ± 0.10
2-site		NMR				Stop Flow			
	Temp [°C]	k_{FU} [s^{-1}]	k_{UF} [s^{-1}]	$k_{FU} + k_{UF}$ [s^{-1}]	p_U [%]	k_{FU} [s^{-1}]	k_{UF} [s^{-1}]	$k_{FU} + k_{UF}$ [s^{-1}]	p_U [%]
	25	46.9 ± 0.5	729 ± 9	776 ± 9	6.04 ± 0.07	55.9 ± 21.1	1038 ± 275	1094 ± 276	5.11 ± 0.59

Table 2S. χ^2 target functions obtained in global fits of CPMG dispersion data for 23(26) residues of G48M(G48V) measured at 5(4) temperatures and 3(2) magnetic fields using 2- and 3-site exchange models (see Methods for details).

		G48M		G48V	
Model	ΔC_P [cal/mol/K]	χ^2	# Degrees of freedom	χ^2	# Degrees of freedom
2-site	0	3883.3	3975	4716.4	2544
	300	3718.0	3975	4658.5	2544
3-site	0	2131.6	3948	1705.7	2514
	300	2050.3	3948	1657.7	2514

Table 3S. Thermodynamic parameters for G48M(G48V) mutants of the Fyn SH3 domain obtained from a global fit of CPMG dispersion data using 3- and 2-site exchange models (see Methods). The rate constants for transitions between F, I and U states are assumed to follow transition state theory. The data were fit with ΔC_p = 0 or 300 cal/mol/K[10] assuming that states IU, I, FI and F have similar levels of compaction so that the change in heat capacity derives from the difference between U and IU (3-site model) or U and UF (2-site model). IU and FI refer to the state of highest energy on the transition from I to U and F to I, respectively (transition states), while UF is the transition state in the 2-site model.

			G48M (at 25.0 °C)			**G48V** (at 17.5 °C)		
	ΔC_p [cal/mol/K]	State	H [kcal/mol]	TS [kcal/mol]	G [kcal/mol]	H [kcal/mol]	TS [kcal/mol]	G [kcal/mol]
3-site	0	F	-17.1 ± 0.3	-14.8 ± 0.2	-2.3 ± 0.02	-6.8 ± 0.3	-4.9 ± 0.2	-1.8 ± 0.01
		FI	2.1 ± 0.5	-11.3 ± 0.5	13.4 ± 0.00	6.1 ± 0.6	-6.9 ± 0.6	13.0 ± 0.02
		I	-13.7 ± 0.5	-14.0 ± 0.5	0.3 ± 0.1	-7.4 ± 0.5	-7.8 ± 0.5	0.4 ± 0.04
		IU	7.9 ± 1.4	-5.1 ± 1.5	13.0 ± 0.1	9.3 ± 1.0	-3.7 ± 1.0	12.9 ± 0.04
		U	0	0	0	0	0	0
	300	F	-15.2 ± 0.3	-12.9 ± 0.2	-2.3 ± 0.02	-5.9 ± 0.3	-4.0 ± 0.2	-1.9 ± 0.02
		FI	3.9 ± 0.5	-9.5 ± 0.5	13.4 ± 0.01	7.1 ± 0.5	-5.9 ± 0.5	13.0 ± 0.02
		I	-11.8 ± 0.5	-12.1 ± 0.5	0.3 ± 0.1	-6.1 ± 0.5	-6.5 ± 0.5	0.4 ± 0.04
		IU	8.8 ± 1.4	-4.2 ±1.4	13.0 ± 0.1	9.9 ± 1.0	-3.0 ± 1.0	12.8 ± 0.04
		U	0	0	0	0	0	0
2-site	0	F	-13.4 ± 0.2	-11.3 ± 0.2	-2.1 ± 0.01	-5.1 ± 0.4	-3.3 ± 0.3	-1.77 ± 0.01
		FU	5.4 ± 0.2	-8.3 ± 0.2	13.8 ± 0.01	8.8 ± 0.5	-4.7 ± 0.4	13.47 ± 0.01
		U	0	0	0	0	0	0
	300	F	-12.2 ± 0.2	-10.1 ± 0.2	-2.1 ± 0.00	-4.3 ± 0.4	-2.6 ± 0.3	-1.8 ± 0.01
		FU	6.8 ± 0.2	-7.00 ± 0.2	13.8 ± 0.01	9.6 ± 0.5	-3.9 ± 0.4	13.5 ± 0.01
		U	0	0	0	0	0	0

Table 4S. Backbone ^{15}N chemical shift differences between states F and I (δ_{FI}) and between states F and U (δ_{FU}) and their ratio $\Delta_{exp}=\delta_{FI}/\delta_{FU}$ for G48M and G48V mutants of the Fyn SH3 domain. The values of δ_{FI} and δ_{FU} were obtained from a global fit of ^{15}N CPMG dispersion data recorded at multiple temperatures for a set of 23(26) residues of G48V (G48M) using a 3-site exchange model, as described in the text (underlined). For the remaining residues δ_{FI} and δ_{FU} were calculated on a per-residue basis with fixed exchange parameters obtained in the global fit (see Fitting of Dispersion Profiles, above). Although the relative signs of δ_{FI} and δ_{FU} are determined from the fits, the absolute signs are not.

Residue	G48M			G48V		
	δ_{FI} [ppm]	δ_{FU} [ppm]	Δ_{exp}	δ_{FI} [ppm]	δ_{FU} [ppm]	Δ_{exp}
Leu 3	0.92	1.17	0.79	0.83	1.19	0.70
Phe 4	-	-	-	1.64	4.87	0.34
Glu 5	4.28	3.05	1.40	1.79	4.27	0.42
Ala 6	-	-	-	2.13	0.20	10.79
Leu 7	6.16	6.19	1.00	1.77	6.47	0.27
Tyr 8	8.36	7.76	1.08	1.72	8.64	0.20
Asp 9	4.51	4.30	1.05	1.43	4.47	0.32
Tyr 10	2.72	2.43	1.12	-	-	-
Glu 11	6.05	6.21	0.98	2.90	6.90	0.42
Ala 12	1.88	2.31	0.81	1.09	2.26	0.48
Arg 13	2.29	1.48	1.55	1.45	1.66	0.87
Thr 14	-	-	-	2.29	5.00	0.46
Glu 15	3.37	3.19	1.06	0.88	3.40	0.26
Ser 19	0.51	1.02	0.50	-	-	-
Phe 20	6.07	6.18	0.98	-	-	-
His 21	2.70	1.65	1.64	1.62	1.69	0.96
Gly 23	5.16	6.62	0.78	1.76	6.38	0.28
Glu 24	2.78	3.67	0.76	0.89	2.44	0.36
Lys 25	-	-	-	2.11	0.80	2.63
Phe 26	3.39	3.27	1.04	0.23	3.33	0.07
Gln 27	1.31	0.49	2.67	-	-	-
Ile 28	1.92	5.23	0.37	-1.04	4.51	-0.23
Leu 29	0.85	2.43	0.35	-0.63	1.98	-0.32
Asn 30	2.31	4.32	0.53	-0.36	3.77	-0.10
Gly 34	-	-	-	-1.04	0.63	-1.65
Asp 35	2.16	1.69	1.28	1.01	1.76	0.58
Trp 36	-	-	-	1.79	0.08	23.17
Trp 37	2.63	2.87	0.92	-0.05	3.21	-0.01
Glu 38	1.52	2.68	0.57	0.26	2.35	0.11
Ala 39	4.20	8.67	0.48	0.87	7.77	0.11
Ser 41	1.24	4.15	0.3	-	-	-
Leu 42	2.09	7.33	0.29	-1.00	6.53	-0.15
Thr 43	3.06	2.82	1.09	-	-	-
Thr 44	2.34	6.79	0.34	-1.07	5.77	-0.19
Gly 45	-	-	-	1.16	0.46	2.54
Glu 46	-	-	-	0.88	0.34	2.60
Thr 47	0.27	2.00	0.13	-0.55	1.94	-0.28
Met/Val 48	-	-	-	2.19	0.15	14.76
Tyr 49	2.05	1.19	1.72	-1.35	3.35	-0.40
Ile 50	10.2	7.95	1.28	1.69	9.39	0.18
Ser 52	-	-	-	1.17	5.30	0.22
Asn 53	1.67	4.55	0.37	-	-	-
Tyr 54	2.51	2.56	0.98	0.95	3.15	0.30
Val 55	15.77	15.22	1.04	2.46	15.68	0.16
Ala 56	8.44	7.96	1.06	2.60	9.23	0.28
Val 58	2.28	1.95	1.17	1.51	1.99	0.76
Asp 59	1.49	0.96	1.55	1.69	1.02	1.65

Figure 1S. Average r.m.s deviation from the native state as a function of residue number for the calculated I states of G48M (left) and G48V (right); the upper and lower limits of the shaded area correspond to the average r.m.s. plus and minus the standard deviation within the ensemble, respectively.

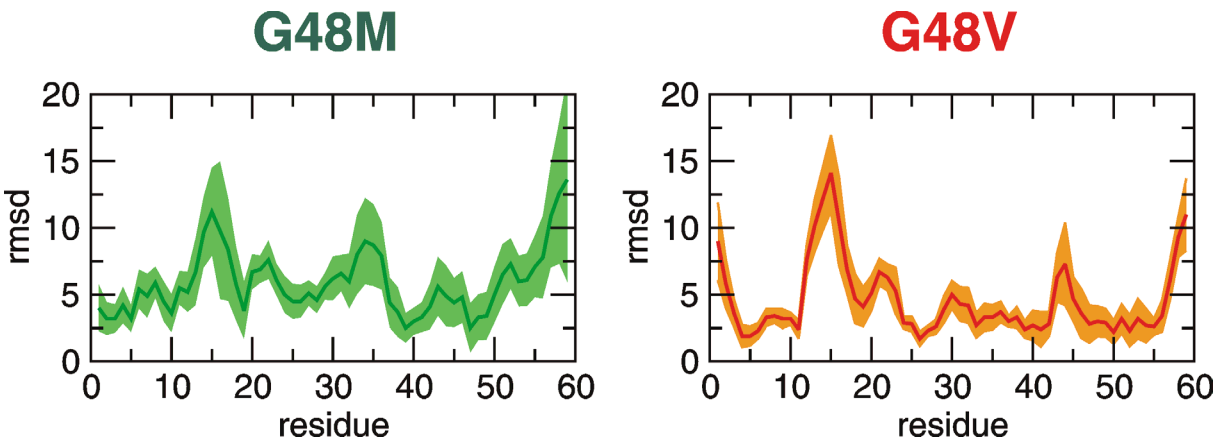

In order to investigate the possibility that the presence of a third state is a consequence of concentration-dependent processes, such as oligomerization of the unfolded state, the relaxation dispersion experiments were repeated for the G48M mutant at a lower concentration (0.3 mM as opposed to 1.0 mM) and at temperatures of 15 and 30^{o}C. The results (Figure 2S, below) show that the populations, rates and chemical shifts, which constitute the output of the analysis of these experiments, are independent of concentration within experimental error. Considering that simulations reveal that these parameters are highly sensitive to the presence of any concentration-dependent process these results indicate that aggregation effects are unlikely to contribute in any significant manner to the analysis presented in this work.

Figure 2S. Relaxation dispersion curves recorded for G48M at concentrations of 1.0 and 0.3 mM, 15 and 30^{o}C, *do not depend on protein concentration*. Dispersion profiles for selected residues, F26, L42 and N53 are indicated with filled (open) squares showing data at 1.0(0.3) mM. The solid red curve through the data points was generated using the exchange parameters k_{FI}=34.0 s^{-1}, k_{IF}=2405 s^{-1}, k_{IU}=5650 s^{-1}, k_{UI} = 2501 s^{-1} (p_F=95.60%, p_I=1.35%, p_U=3.05%) (Table 1S) and $\Delta\omega$ values (Table 4S) extracted from global fits of all dispersion data (1.0 mM protein concentration) as described in Methods, assuming the U$\leftrightarrow$I$\leftrightarrow$F folding model (used in the paper). Several other models have been investigated, including:

(1) $U_2 \leftrightarrow 2U \leftrightarrow 2F$

(2) $2U \leftrightarrow U_2 \leftrightarrow 2F$

(3) $U_2 \leftrightarrow I_2 \leftrightarrow 2F$

Using the values of k_{ij} listed above and values of $\Delta\omega$ extracted on a per-residue basis (see Figure 1S and Table 4S) dispersion curves have been calculated for F26, L42 and N53 assuming models (1-3) and a total protein concentration of 0.3 mM. The calculated dispersion profiles are shown in Figure 1S (bottom three traces, solid lines) and they clearly differ from the experimental dispersions recorded on the 0.3mM sample. Thus, models of dimerization (or for that matter higher oligomerization) of either U or I can be discarded. In a similar manner it can be shown that models which assume that F oligomerizes and that this is responsible for the experimental dispersion profiles can also be discarded.

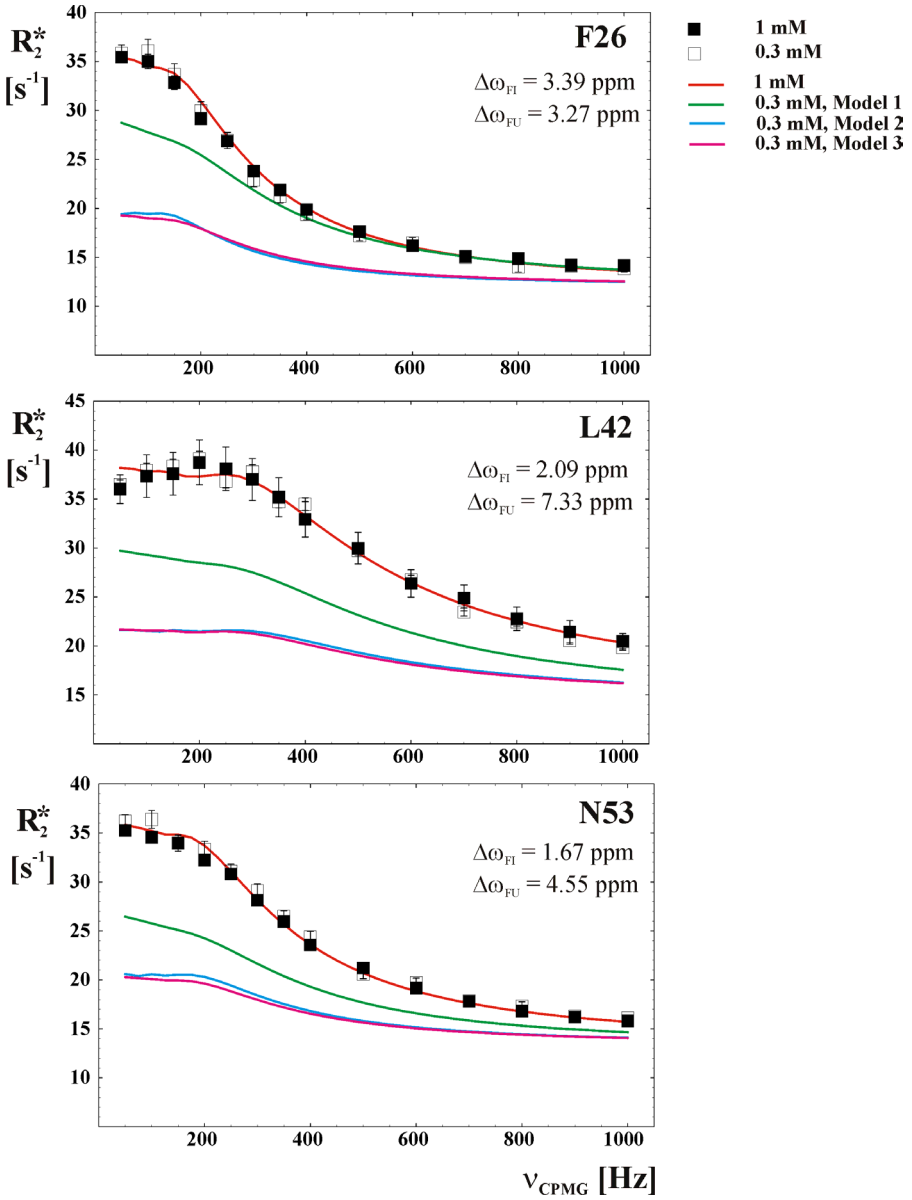

References

1. Tollinger, M., Skrynnikov, N. R., Mulder, F. A. A., Forman-Kay, J. D. & Kay, L. E. Slow dynamics in folded and unfolded states of an SH3 domain. *J. Am. Chem. Soc.* **123**, 11341-11352 (2001).

2. Millet, O., Loria, J. P., Kroenke, C. D., Pons, M. & Palmer, A. G. The static magnetic field dependence of chemical exchange linebroadening defines the NMR chemcial shift time scale. *J. Am. Chem. Soc.* **122**, 2867-2877 (2000).

3. Zar, Z. H. *Biostatistical Analysis* (Prentice-Hall Inc., Englewood Cliffs, N.J., 1984).

4. Press, W. H., Flannery, B. P., Teukolsky, S. A. & Vetterling, W. T. *Numerical Recipes in C* (Cambridge University Press, Cambridge, 1988).

5. Noble, M. E., Musacchio, A., Saraste, M., Courtneidge, S. A. & Wierenga, R. K. Crystal structure of the SH3 domain in human Fyn; comparison of the three-dimensional structures of SH3 domains in tyrosine kinases and spectrin. *Embo J* **12**, 2617-2624. (1993).

6. Schaftenaar, G. & Noordik, J. H. Molden: a pre- and post-processing program for molecular and electronic structures. *J. Comput.-Aided Mol. Design* **14**, 123-134 (2000).

7. Brooks, B. R. *et al.* CHARMM: a program for macromolecular energy minimization and dynamics calculations. *J. Comput. Chem.* **4**, 187-217 (1983).

8. Xu, X. P. & Case, D. A. Probing multiple effects on ^{15}N, $^{13}C\alpha$, $^{13}C\beta$, $^{13}C'$ chemical shifts in peptides using density functional theory. *Biopolymers* **65**, 408-423 (2002).

9. Paci, E. & Karplus, M. Forced unfolding of fibronectin type 3 modules: an analysis by biased molecular dynamics simulations. *J. Mol. Biol.* **2888**, 441-459 (1999).

10. Di Nardo, A. A., Korzhnev, D., Zarrine-Afsar, A., Kay, L. E. & Davidson, A. R. Dramatic acceleration of protein folding by stabilization of a non-native backbone conformation. *Proc. Natl. Acad. Sci. USA In Press*.